Stem Cell Reports
Article

ISSCR

OPEN ACCESS

Isolation and Mechanical Measurements of Myofibrils from Human Induced Pluripotent Stem Cell-Derived Cardiomyocytes

Josè Manuel Pioner,[1,*] Alice W. Racca,[2] Jordan M. Klaiman,[2] Kai-Chun Yang,[3] Xuan Guan,[4] Lil Pabon,[5] Veronica Muskheli,[5] Rebecca Zaunbrecher,[2] Jesse Macadangdang,[2] Mark Y. Jeong,[6] David L. Mack,[4,7] Martin K. Childers,[4,7] Deok-Ho Kim,[2] Chiara Tesi,[1] Corrado Poggesi,[1] Charles E. Murry,[2,3,5,7,8] and Michael Regnier[2,7,8]

[1]Division of Physiology, Department of Experimental and Clinical Medicine, University of Florence, Viale Morgagni 63, 50134 Florence, Italy
[2]Bioengineering, University of Washington, Seattle, WA 98109, USA
[3]Medicine, Division of Cardiology, University of Washington, Seattle, WA 98195, USA
[4]Rehabilitation Medicine, University of Washington, Seattle, WA 98109, USA
[5]Pathology, University of Washington, Seattle, WA 98109, USA
[6]Medicine, Division of Cardiology, University of Colorado, Denver, CO 80262, USA
[7]Institute for Stem Cell and Regenerative Medicine, University of Washington, Seattle, WA 98109, USA
[8]Center for Cardiovascular Biology, University of Washington, Seattle, WA 98109, USA
*Correspondence: jose.pioner@unisi.it
http://dx.doi.org/10.1016/j.stemcr.2016.04.006

SUMMARY

Tension production and contractile properties are poorly characterized aspects of excitation-contraction coupling of human induced pluripotent stem cell-derived cardiomyocytes (hiPSC-CMs). Previous approaches have been limited due to the small size and structural immaturity of early-stage hiPSC-CMs. We developed a substrate nanopatterning approach to produce hiPSC-CMs in culture with adult-like dimensions, T-tubule-like structures, and aligned myofibrils. We then isolated myofibrils from hiPSC-CMs and measured the tension and kinetics of activation and relaxation using a custom-built apparatus with fast solution switching. The contractile properties and ultrastructure of myofibrils more closely resembled human fetal myofibrils of similar gestational age than adult preparations. We also demonstrated the ability to study the development of contractile dysfunction of myofibrils from a patient-derived hiPSC-CM cell line carrying the familial cardiomyopathy *MYH7* mutation (E848G). These methods can bring new insights to understanding cardiomyocyte maturation and developmental mechanical dysfunction of hiPSC-CMs with cardiomyopathic mutations.

INTRODUCTION

Methods to mature human induced pluripotent stem cell-derived cardiomyocytes (hiPSC-CMs) may provide considerable advantages to model inherited cardiac diseases in culture (Eschenhagen et al., 2015; Jung and Bernstein, 2014; Yang et al., 2014a). Early-stage hiPSC-CMs lack discernible T tubules, display rhythmic spontaneous beating with short action potential duration and slow, diffusion-limited calcium influx (Lundy et al., 2013). In addition, the contractile machinery of hiPSC-CMs is typically sparse and poorly organized (Gherghiceanu et al., 2011; Kamakura et al., 2013; Lundy et al., 2013). Measuring tension remains one of the least characterized aspects of excitation-contraction coupling (ECC), due to the small size and structural immaturity of hiPSC-CMs. Thus, developing methods to measure the contractile properties of hiPSC-CMs and their subcellular organelles, myofibrils, could improve our knowledge of how early-stage cardiomyocytes function during fetal development and at the earliest stages of heart disease.

In multicellular preparations, such as engineered heart tissue constructs, contractile tension of hiPSC-CMs propagates from cell to cell, and tension generation is in the order of micronewtons/section (Tulloch et al., 2011). However, low cell density, sparse cell-cell coupling, and the compliance of hydrogel- or protein-based scaffolds likely underestimates tension generation and affect contractile kinetics measurements. Single hiPSC-CM tension has been estimated by contraction stress assays (Ribeiro et al., 2015) or atomic force microscopy (Liu et al., 2012; Sun et al., 2012) but at dissimilar post-differentiation times. Moreover, two-point force assays detect twitch properties along a single axis and do not include lateral stresses, including friction due to the culture surface. Individual cardiomyocytes cultured on micropost arrays (Rodriguez et al., 2011, 2014; Yang et al., 2014b) can obviate this gap by measuring the tension, velocity, and power of contraction for subcellular bundles of myofibrils at each adhesion point. However, culturing hiPSC-CMs on micropost arrays limits myofibril elongation and bundling, cell morphology maintains a high circularity index, and the resultant tension is the sum of the contraction of unaligned myofibrils developed in multiple directions.

Myofibrils are the smallest subunit of the cardiomyocyte contractile apparatus and consist of sarcomeres (single contractile units) in series. Here we present a method to

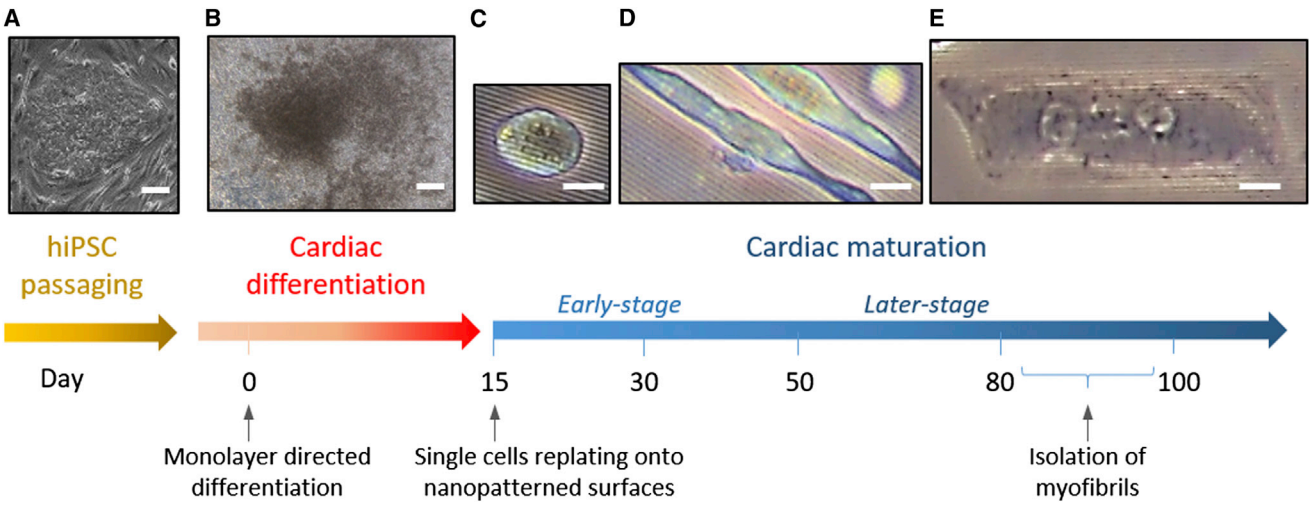

Figure 1. Protocol for Cardiac Maturation of Human Pluripotent Stem Cells on Nanopatterned Surfaces in Long-Term Cultures

(A–E) Phase-contrast images of hiPSCs at different stages of differentiation and cardiac maturation. (A) hiPSC passaging before differentiation. (B) At day 0, hiPSCs were differentiated into cardiomyocytes with a monolayer-directed differentiation protocol. Beating areas were visible from day 8 post-differentiation (p.d.). (C) At 15 p.d, single hiPSC-CMs were replated onto nanopatterned surfaces until day 80–100 in low density for cardiac maturation. Early-stage hiPSC-CMs were round-shaped and lacked of aligned myofibrils. (D) After replating, hiPSC-CMs showed early progressive elongation and increased myofibril density/alignment. (E) Later-stage hiPSC-CMs were rod-shaped and myofibrils were highly aligned. These cells had length of 127.3 ± 8.8 μm and width of 14.7 ± 0.9 μm (n = 44 from controls). Scale bars in (A) and (B) represent 200 μm; scale bars in (C), (D), and (E) represent 20 μm.

measure the mechanical properties of single myofibrils isolated from hiPSC-CMs by a fast solution switching method (Colomo et al., 1998) that represents a unique tool to assess both steady-state tension and kinetics of contraction and relaxation, independent of the Ca^{2+} handling properties of the cells. The biochemical milieu surrounding myofibrils can easily be controlled experimentally to provide mechanistic insights on actin-myosin cross-bridge cycling and regulation of tension development and relaxation kinetics. Mechanical properties of myofibrils from hiPSC-CMs have not previously been investigated due to their small size and fragility in culture. To overcome this limitation, we developed strategies to drive cardiomyocyte morphology toward an adult phenotype. Single cardiac cells were seeded at low density onto nanopatterned surfaces (Kim et al., 2010; Macadangdang et al., 2014, 2015) and cultured long term (Lundy et al., 2013). This resulted in cell elongation and myofibril bundling, demonstrated by Z bands across the entire cell width and length. Cells had increased myofibril density with evidence of T-tubule formation. We then isolated hiPSC-CM functional myofibrils from nanopatterned cultures to study their contractile properties. We used this system to compare hiPSC-CM myofibrils with those from fetal and adult hearts and to demonstrate impaired myofibril mechanics from a patient-derived line harboring a cardiomyopathic mutation (E848G) in β-myosin heavy chain (*MYH7*).

RESULTS

Engineering hiPSC-CM Morphology

hiPSC-CMs were generated from cells collected either from urine ($control_1$) (Guan et al., 2014) or skin fibroblasts ($control_2$; FCM) using directed differentiation of high-density monolayers with a combination of activin A and BMP4, along with small molecules that sequentially activate and repress Wnt/β-catenin signaling (Palpant et al., 2015) (Figures 1A and 1B). At 15–20 days post-differentiation (p.d.), single hiPSC-CMs were replated at low density onto fibronectin-coated nanopatterned surfaces fabricated with parallel grooves and ridges of 800 nm width and spacing to promote cell spreading (Kim et al., 2010). Just after replating, 15–20 days p.d. hiPSC-CMs were round-shaped and demonstrated sporadic signs of myofibrillogenesis with sparse expression of sarcomeric elements and assembly in fieri (Figures 1C and 5A, top). Obtaining mechanical measurements from these pre-myofibrils is quite challenging due to their short length and fragility. Therefore, to achieve myofibril lengths (>50+ μm) and stability that would enable us to obtain mechanical measurements on our experimental platform, hiPSC-CMs were cultured for an additional 60 days on nanopatterned surfaces (80–100 days p.d. total). This resulted in cells that were elongated (Figure 1D), and many had dimensions similar to those found for cultured adult cardiomyocytes

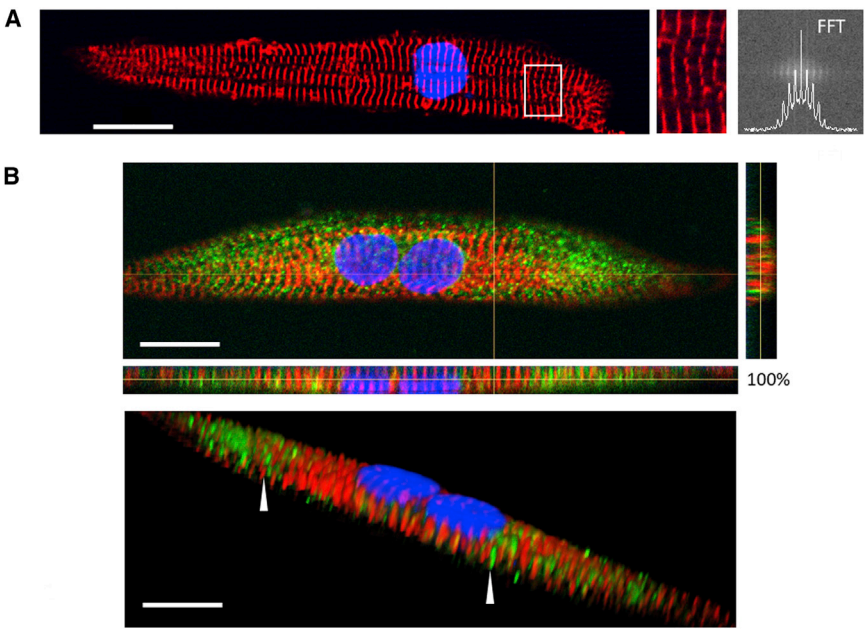

Figure 2. Later-Stage hiPSC-CMs Grown on a Nanopatterned Surface Promote Myofibril Alignment and T-Tubule Formation

(A) Confocal images of later-stage hiPSC-CMs grown on nanopatterned surfaces. Cells were stained for Z bands (α-actinin, red) and for nuclei (DAPI, blue). hiPSC-CMs exhibited mature morphology with rod-shaped, aligned myofibrils and clearly defined Z bands (enlargement of the area within the white rectangle) as quantified by fast Fourier transform (FFT) analysis.

(B) Confocal images of hiPSC-CMs stained with antibody against caveolin-3 (green), α actinin (red), and nuclei (blue). Top: hiPSC-CMs displayed development of a transverse-axial tubular system (TATS), with both transverse and axial elements. Bottom: representative 3D picture of TATS in hiPSC-CMs. Arrowheads in the 3D reconstruction highlight transverse tubular elements (green), running in parallel to a Z line (red). Axial tubules occurred perpendicularly to the Z lines and were evident in the side view. Scale bars represent 20 μm.

(Figure 1E). Cells were rod-shaped with average lengths of 127.3 ± 8.8 μm and average widths of 14.7 ± 0.9 μm. In all hiPSC-CMs, myofibril alignment followed the nanotopographic pattern.

Adult-like Morphology and Dimensions of Later-Stage hiPSC-CMs

Later-stage hiPSC-CMs (80–100 days p.d. total; Figure 1E) were stained for Z bands (anti α-actinin). As observed by phase-contrast imaging (Figure 2A), quantitative immunocytochemical analysis demonstrated later-stage control-hiPSC-CMs were characterized by aligned myofibrils and clearly defined Z bands spanning the width of the cells. We used fast Fourier transform analysis to quantify the myofibril alignment index based on the regularity of Z bands. Later-stage hiPSC-CMs (Figure 2) had an extended cell area (control = 7,696 ± 519 μm^2) and perimeter (control = 291 ± 11 μm) with an elevated index of myofibril alignment (control = 0.014 ± 0.002), indicating a high impact on myofibril organization with this combinatorial approach for cardiomyocyte maturation.

We further investigated the cell structure by staining for caveolin-3 (CAV3), a scaffolding protein of the sarcolemma, which is associated with the formation of caveolae and T tubules during the development of striated muscle (Parton et al., 1997). CAV3 is also implicated in several electromechanical regulation pathways (Gazzerro et al., 2010). Top and side views of confocal images (Figure 2B) display the organization of cells co-stained for CAV3 and Z bands. In a 3D reconstruction of the confocal images, the cells had a homogeneous distribution of CAV3 over the entire sarcolemma. CAV3 staining revealed finger-like invaginations tightly associated with Z bands, likely representing transverse (T)-tubule-like structures during development (Pasek et al., 2008). This finding provides evidence that transverse-axial tubular system (TATS) formation may occur together with myofibrillogenesis and suggests a strict interplay between tubules and Z bands during cardiac development on nanopatterned surfaces.

Isolation of Myofibrils from hiPSC-CMs

The improved cell morphology and size of later-stage cardiomyocytes cultured on nanopatterned surfaces allowed us to obtain isolated myofibrils with sufficient length and stability for detailed contractile analysis. To isolate myofibrils, we modified a procedure we have commonly used to obtain myofibrils from cardiac tissue. This method is demonstrated in Figure 3A. We examined two cell skinning approaches to harvest myofibrils: (1) cultured hiPSC-CMs were subjected to pre-treatment with a Rho-associated protein kinase inhibitor (ROCKi) for 1 hr to promote cell detachment and prevent the anoikis phenomena. Cells were subsequently detached by treatment with Versene for 1 hr. hiPSC-CMs were collected from the supernatant and rapidly skinned in rigor solution containing Triton X-100 buffer (1%) for 10 min (skinning in suspension; Figure 3A (1)). Triton X-100 was then removed by two sequential rinses in normal rigor solution. Versene treatment is

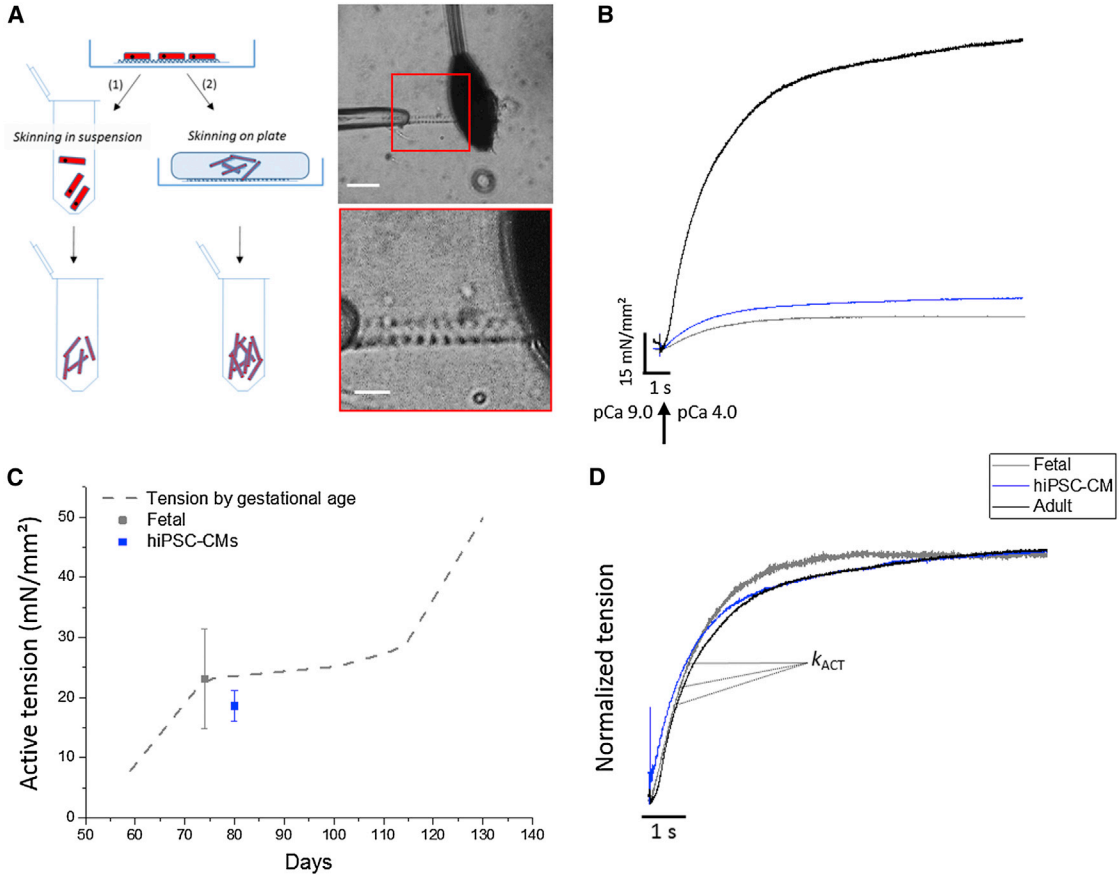

Figure 3. Isolation, Tension Generation, and Kinetic Properties of hiPSC-CM Myofibrils

(A) Scheme for the isolation of myofibrils from hiPSC-CMs. Two skinning approaches were developed. (1) Skinning in suspension: myofibril density in the final suspension was variable and limited by the efficiency of cell detachment. (2) Skinning on plate: myofibril density in the final suspension was significantly higher. Right: representative phase-contrast images of a thin bundle of myofibrils from hiPSC-CMs, collected with the latter method at different magnifications. Myofibrils were mounted between the tip of a length controller (left) and a calibrated cantilever (right) in a custom-built apparatus. Myofibril mechanics and kinetics were measured by fast solution switching.

(B) Representative traces of tension generation of hiPSC-CM (blue), human ventricular fetal (fetal, gray) and adult (black) myofibrils maximally activated. Compared with adult, both fetal and hiPSC-CM myofibril isometric maximal tension (pCa 4.0) was weaker.

(C) Dashed line represents the line fit to the data (N > 3 and n = 4–40 per condition) from Racca et al. (2015) of how tension-generating capacity developed with increasing gestational age of human fetal ventricular samples (Racca et al., 2015). hiPSC-CM (80 days p.d., blue) myofibrils generated the same maximal tension as those of human fetal ventricle at a similar gestational age (74 days gestation, gray).

(D) Following Ca^{2+} application, force developed exponentially with a rate constant (k_{ACT}) that reflects the cross-bridge turnover rate. In hiPSC-CM myofibrils, kinetics of activation were in the same order of magnitude. Data from human fetal and adult cardiac myofibrils are reported in Racca et al. (2015). Experimental conditions: 15°C; pCa relaxing and activating solution, 9.0 and 4.0, respectively.

gentle and helps to retain intact cell architecture throughout the skinning process. The limiting aspect of this approach is the efficiency of cell detachment, which can affect myofibril density in the final suspension. (2) The second approach consisted of skinning hiPSC-CMs in rigor solution with 1% Triton X-100 applied directly on culture plates for 5 min (skinning on plate; Figure 3A (2)). The quality of viable myofibrils obtained with the two approaches was indistinguishable, as determined by the morphological and contractile properties, however the yield of myofibrils was substantially greater with the second approach. Thus, we used the second method to obtain isolated single and small bundles of myofibrils (Figure 3A right) to assess the contractile properties of all hiPSC-CM lines.

Mechanical and Kinetic Properties of Myofibrils from hiPSC-CMs

Figures 3B and 4A illustrate representative tension traces of myofibrils from later-stage hiPSC-CMs maximally activated

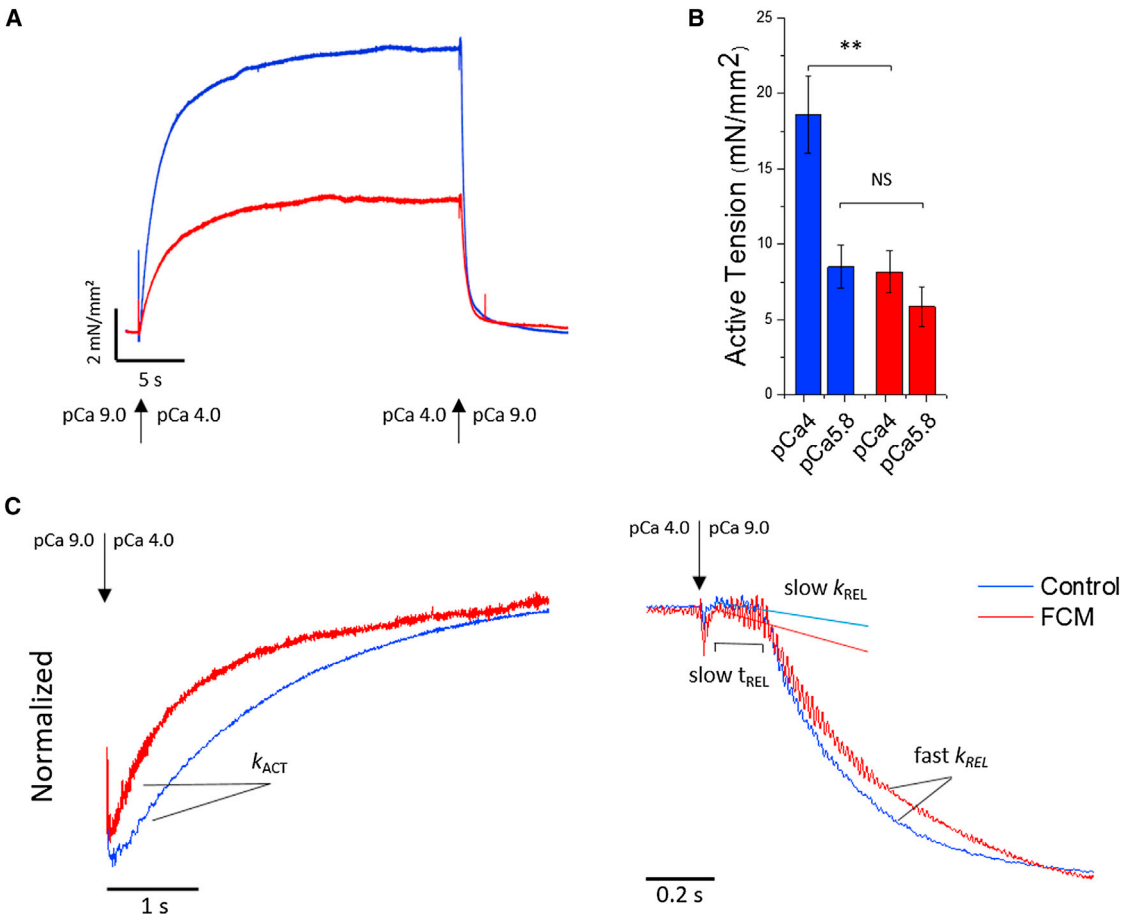

Figure 4. Tension Generation and Kinetic Properties of Control and FCM-hiPSC-CM Myofibrils

(A) Representative traces of tension generation of control (blue) and FCM-CM (red) myofibrils maximally activated and fully relaxed by the fast solution switching method.

(B) Compared with controls, FCM-CMs myofibril isometric maximal tension (pCa 4.0) is impaired. At submaximal Ca^{2+} level (pCa 5.8), tension generation was reduced 50% in control but only 28% in FCM, indicating increased Ca^{2+} sensitivity of tension development (N > 3 and n = 15–26 per condition).

(C) Left: following Ca^{2+} application, tension develops exponentially with a rate constant (k_{ACT}). Right: the reversed movement of the pipette induced biphasic relaxation. In the slow linear phase (rate, slow k_{REL} and duration slow t_{REL}), force decay occurred under isometric conditions and in the absence of Ca^{2+}. The fast exponential phase (rate, fast k_{REL}) follows sarcomere "give" and reflects inter-sarcomere dynamics. FCM-CM myofibrils exhibited faster k_{ACT}, indicating an accelerated cross-bridge turnover rate. Slow k_{REL} was faster with no difference in slow t_{REL}. The fast monoexponential phase of relaxation (fast k_{REL}) was slower.

Averages in (B) are reported as means ± SEM; data shown refer to Table 1; **p < 0.01; NS not significant estimated by Student's t test.

(15°C) by rapid solution switching, via a double-barreled perfusion pipette, from low Ca^{2+} (pCa9) to high Ca^{2+} (pCa4) (Racca et al., 2015). With activation, tension developed exponentially with a rate constant (k_{ACT}; Figures 3D and 4C) that reflects thin filament activation upon Ca^{2+} binding, the rate of strong myosin binding to actin (cross-bridge formation), the subsequent force-generating cross-bridge isomerization and initial cross-bridge turnover. The inverse movement of the perfusion pipette results in rapid Ca^{2+} removal from the solution flow, subsequently resulting in an initial slow, linear phase of relaxation followed by rapid relaxation to baseline tension. During the slow phase of relaxation, force decay occurs under isometric conditions with a rate constant (slow k_{REL}; Figure 4C) reflecting the rate of cross-bridge detachment, independent of Ca^{2+} dissociation from troponin C. The subsequent fast monoexponential phase of relaxation (fast k_{REL}; Figures 4A and 4C) is associated with sarcomere "give" and reflects inter-sarcomere dynamics (Poggesi et al., 2005). Maximal and submaximal (pCa5.8) isometric tension and the kinetic properties of myofibrils from hiPSC-CM cell lines were obtained from two healthy adults. $Control_1$- and

Table 1. Summary of Mechanical and Kinetic Properties of Myofibrils From hiPSC-CMs Following Maximal and Submaximal Ca^{2+} Activation

Myofibril Type[a]	Tension (mN/mm^2)[b]	k_{ACT} (s^{-1})[c]	k_{REL}, Slow (s^{-1})[d]	t_{REL}, Slow (ms)[e]	k_{REL}, Fast (s^{-1})[f]
pCa 4.0[g]					
Control (n)	18.6 ± 2.5 (26)	0.51 ± 0.04 (23)	0.30 ± 0.04 (25)	192 ± 7.4 (29)	2.66 ± 0.3 (25)
FCM (n)	8.2 ± 1.4 (15)**	0.83 ± 0.13 (14)*	0.37 ± 0.09 (13)	191 ± 21 (13)	1.69 ± 0.3 (15)*
pCa 5.8[h]					
Control (n)	8.5 ± 1.4 (22)	0.39 ± 0.06 (22)	0.30 ± 0.03 (17)	154 ± 7.9 (21)	2.47 ± 0.4 (22)
FCM (n)	5.9 ± 1.3 (14)	0.40 ± 0.04 (13)	0.58 ± 0.12 (15)*	186 ± 17 (14)	2.07 ± 0.4 (15)

*$p < 0.05$; **$p < 0.01$; estimated by Student's t test.
[a]Data are means ± SEM. For the comparison with FCM myofibrils, $control_1$ and $control_2$ data were merged. N = 3 for each condition.
[b]Tension, maximal, and submaximal Ca^{2+}-activated tension.
[c]Rate of force generation following Ca^{2+}-activation.
[d]Slow, rate of the slow isometric phase of relaxation estimated from the normalized slope of the linear fit to the force trace.
[e]Slow, duration of the slow isometric phase of relaxation following sudden Ca^{2+} removal.
[f]Fast, rate of the fast phase of relaxation estimated from the time constant of the exponential fit to the force trace.
[g]Maximal activating solution.
[h]Submaximal activating solution.

$control_2$-hiPSC-CMs were highly comparable in the magnitude and development of maximal tension (k_{ACT}, pCa4) and relaxation parameters (slow k_{REL}, slow t_{REL}, and fast k_{REL}) (Table S1). Thus, we merged the two datasets for all subsequent comparisons (Table 1).

In order to characterize myofibril mechanics and kinetics from hiPSC-CMs, we sought to compare these contractile properties with similar measurements from human fetal and adult cardiac myofibrils, reported recently by our group (Belus et al., 2010; Piroddi et al., 2007; Racca et al., 2015). Figure 3C shows representative tension traces from hiPSC-CMs versus fetal (74 days gestational) and adult myofibrils. Isometric tension generation of hiPSC-CM myofibrils was about 6-fold less than adult human ventricular (Piroddi et al., 2007) or atrial myofibrils (Belus et al., 2010), and about 5-fold less compared with failing human myocardium (Moussavi-Harami et al., 2015; Racca et al., 2015). However, myofibril tension was comparable with our recent report on human fetal ventricular myocardium of a similar age (Racca et al., 2015). Figures 3B and 3C shows that later-stage hiPSC-CM tension (80 days p.d.) closely matches age-related progression of increasing tension of human cardiac tissue in utero. In contrast to tension production, the kinetics of activation and relaxation for hiPSC-CM myofibrils was similar to what we have previously reported for adult and fetal myofibrils (Figure 3D), indicating related acto-myosin kinetics at this stage. This may be primarily due to all three myofibril groups having β-MHC as the predominant contractile motor isoform (see below). Thus, our data indicate that the magnitude of myofibril tension production is a more valid yardstick for estimating maturation of cardiac myofibrils than parameters of activation and relaxation kinetics. In addition, even though later-stage hiPSC-CMs are beginning to resemble adult cardiomyocyte morphology, our data indicate that the maturation state of individual myofibrils more closely matches gestational development of fetal ventricular muscle.

Modeling Development of Contractile Dysfunction with Familial Cardiomyopathy Mutations

To test the feasibility of using hiPSC-CMs to study the development of contractile abnormalities for disease-associated mutations in sarcomere proteins, we compared age-matched FCM-hiPSC-CMs (FCM) carrying the mutation E848G in β-MHC differentiated and cultured under the same conditions as controls (control-CMs). FCM-hiPSCs were generated from a family showing a unique familial cardiomyopathy that appeared with relatively early onset of arrhythmias, systolic and diastolic dysfunction, without changes in chamber size and wall/septal thickness, suggesting a non-hypertrophic phenotype. Compared with control-CMs, FCMs had increased cell area ($p < 0.01$) and cell perimeter ($p < 0.05$) (Figure S1). Fast Fourier transform quantitative analysis of the FCM myofibril alignment index indicated myofibril disarray throughout the cytoplasm of some but not all FCMs, compared with consistent control-CM myofibril alignment, presenting a puzzling variability for the FCM cells ($p < 0.01$). Despite this dramatic difference in myofibril organization, resting sarcomere length (the distance between Z bands within a myofibril) was comparable with control-CMs ($p = 0.71$).

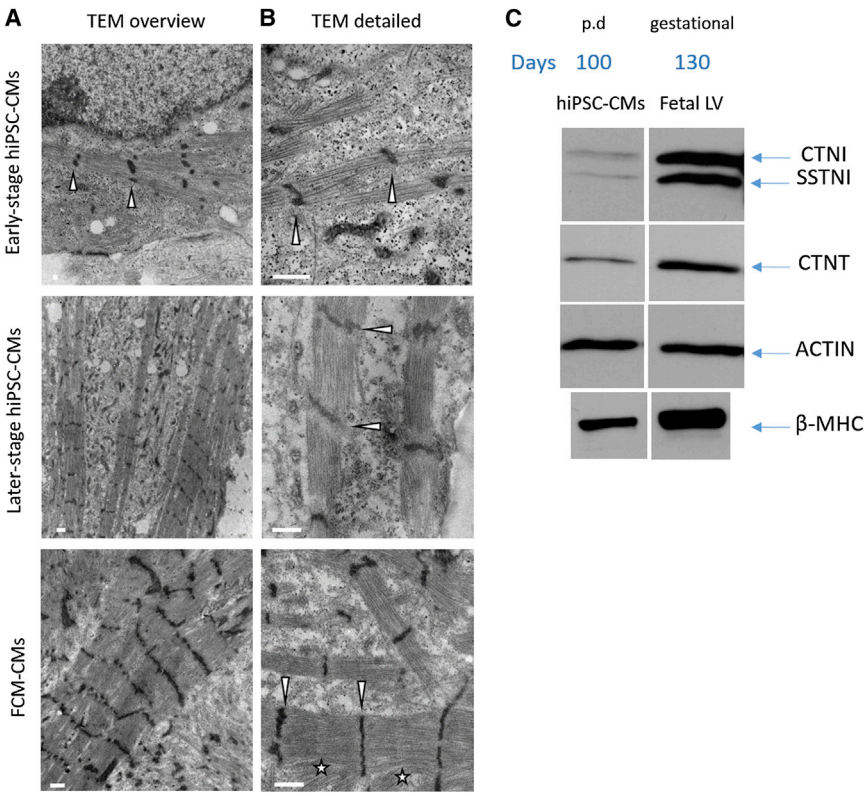

Figure 5. Ultrastructural Organization and Proteomics of Later-Stage hiPSC-CMs on Nanopatterned Surfaces Reveal Immature Sarcomeric Composition

Single cells in sparse cultures on nanopatterned surfaces were investigated for sarcomeric ultrastructures.

(A) Transmission electron microscopy (TEM) images of early-stage ($control_1$), later-stage ($control_1$), and FCM-hiPSC-CMs (FCM-CMs) at low magnification (12,000×) show the presence of aligned myofibrils. Early stages look quite immature with contractile machinery forming but early occurrence of myofibril alignment. Later stages (both control and FCM-CMs) were more mature showing bundling of Z bands (arrowheads).

(B) TEM images acquired at higher magnification (40,000×) confirm a clear alignment of Z disks (arrowheads), but variable-spaced thick filaments remarkably visible in FCM-hiPSC-CMs with evidence of myofibril disarray in some cases. Both later-stage cell lines expressed I-Z-I bands with no clear evidence of H zones. In FCM-CMs, the sarcomeric ultrastructure was highly variable with sparse expression of M lines (stars).

(C) Proteomics of later-stage hiPSC-CMs (100 days p.d.) were compared with fetal left ventricular (LV) samples (130 gestational days). β-myosin was predominant at this stage of maturation indicating α to β isoform switch has occurred. CTNI expression indicated a higher grade of maturation. However, SSTNI was still expressed, confirming immature phenotype as seen for fetal LV. Representative western blot images were cropped. Scale bars represent 1 μm for the overview and 500 nm for the detailed view.

In addition, the CAV3 expression profile was similar for both cell lines with analogous distribution throughout the sarcolemma (Figure S2).

Representative traces (Figure 4A) demonstrate marked impairment of maximal isometric tension generation for FCM myofibrils ($p < 0.01$; Figure 4B and Table 1). We also measured tension at a submaximal Ca^{2+} level (pCa 5.8), closer to where the heart operates. At pCa 5.8, tension generation was approximately half maximal for control-CM myofibrils, but about 0.72 of maximal tension for FCM myofibrils (Figure 4B and Table 1). This suggests that FCM myofibrils had increased Ca^{2+} sensitivity of tension development (Figure 4B), as reported for other hypertrophic cardiomyopathy mutations (Poggesi and Ho, 2014).

During maximal activation, k_{ACT} was faster ($p < 0.05$) for FCM myofibrils (Figure 4C and Table 1), suggesting an increased rate of acto-myosin cross-bridge turnover. As expected, at submaximal Ca^{2+} levels, k_{ACT} was slower than for maximal (pCa 4.0) activations (Table 1). However, in contrast to maximal k_{ACT} (Figure 4C and Table 1), there was no difference in k_{ACT} at pCa5.8 ($p = 0.83$). There were also differences in the relaxation kinetic parameters. Slow k_{REL} (Figure 4C and Table 1) was faster for FCM myofibrils but the difference was significant only for submaximal activation (pCa4.0, $p = 0.25$; pCa5.8, $p < 0.05$), a finding that supports the hypothesis that the cross-bridge detachment rate is increased (Figure 4C and Table 1). The cross-bridge detachment rate is one determinant of the cross-bridge turnover rate, suggesting that the E848G β-MHC mutation may increase cross-bridge turnover by accelerating cross-bridge detachment. This could at least partially explain the lower tension-generating capacity of FCM myofibrils. Finally, there was also a difference in fast k_{REL}, which was slower for FCM myofibrils during maximal activation ($p < 0.05$). This may be a consequence of the increased myofibril Ca^{2+} sensitivity (Kreutziger et al., 2011; Stehle et al., 2009).

Myofibril Ultrastructural and Proteomics

Longitudinal sections of single hiPSC-CMs sparsely cultured onto nanopatterned surfaces were analyzed by transmission electron microscopy (TEM). Images of control- and FCM-CMs clearly demonstrate myofibril alignment (Figure 5A), previously based on Z-band staining

(Figures 2A and S1). Although morphological analysis by confocal images may suggest adult-like cell characteristics, the ultrastructural architecture of myofibrils demonstrated variable-spaced thick filaments that frequently had a paucity of sarcomeric determinants. Both cell lines expressed I-Z-I bands, although no evidence of H zones was identified (Figure 5B). In FCM-CMs, the variable phenotype of the sarcomeric ultrastructure appeared more pronounced within cells, with sparse expression of M lines (Figure 5B).

Western blot analysis of myosin isoform composition indicated a significant amount of β-MHC present in control and FCM myofibrils, suggesting that the myosin isoform switch likely began prior to this stage of maturation (Figure 5B). This agrees well with our recent report that fetal cardiac myofibrils contain β-myosin predominantly as early as 74 days gestation (Racca et al., 2015), which, in turn, agrees with reports by others (Reiser et al., 2001). These data also suggest that differences in contractile kinetics between control and FCM myofibrils were not the result of the myosin isoform, suggesting that they were likely due to the E848G mutation. Troponin I (TNI) isoforms can be used as an indicator of maturation. Early in development, cardiomyocytes express slow skeletal TnI (SSTNI). As maturation proceeds, the cardiac isoform of TNI begins to be expressed and later in development becomes the predominant isoform (Racca et al., 2015; Sasse et al., 1993). Control- and FCM-CMs expressed both TNI isoforms (Figure 5C) indicating that the maturation state of the myofibrils was more similar to fetal left ventricular myofibrils than adult (which express CTNI exclusively), consistent with other hiPSC-CMs cultured over time (Bedada et al., 2014).

DISCUSSION

In this study, we report that hiPSC-CMs on nanogrooved surfaces in long-term culture can achieve a high degree of structural maturation. Previous reports concluded that T tubules in 2D culture are nearly absent in hiPSC-CMs (Jung and Bernstein, 2014; Yang et al., 2014a). Here, hiPSC-CMs demonstrated clear evidence of a complex architecture that may be associated with forming TATS, and this should be further explored (Sacconi et al., 2012). TATS is an important hallmark for ECC regulation, with well-aligned Z bands together with composition of elongated myofibrils. We isolated functional myofibrils from these later-stage hiPSC-CMs using a cell skinning method and used a custom-built apparatus (Kreutziger et al., 2011; Racca et al., 2015) to measure maximal and submaximal myofibril tension generation that was considerably greater than values from previous reports in intact hiPSC-CMs (Ribeiro et al., 2015; Rodriguez et al., 2014; Sun et al., 2012). Our values demonstrate weaker force compared with adult cardiac myofibrils but, interestingly, very similar to what we recently reported for human fetal myofibrils of similar gestational age (Racca et al., 2015). Thus, the morphological maturation of later-stage hiPSC-CMs was not matched by maturation of myofibril contractile properties, suggesting that caution should be used when reporting the maturation state by limited analytical criteria.

This study represents a solid step forward in the study of hiPSC-CM development, and it further demonstrates its utility to model the development of disease-related cardiomyocyte contractile dysfunction. First, we may have established features of in vivo gestational maturation in an in vitro model, as indicated from our comparisons with fetal cardiac myofibrils. Second, we may now consider myofibril tension and kinetics of contraction and relaxation as parameters to quantitatively assess maturation state of hiPSC-CM contractile machinery. Others have reported high similarities between hiPSC-CMs and human fetal cardiomyocytes in the gene expression profile (Kuppusamy et al., 2015; Synnergren et al., 2012; van den Berg et al., 2015), structural composition (Gherghiceanu et al., 2011; Kamakura et al., 2013; Lundy et al., 2013), and electrophysiological and contractile properties (Ribeiro et al., 2015). However, to our knowledge, no other study has quantified the maturation stage of hiPSC-CMs in comparison with fetal cardiomyocyte development. We observed ultrastructural features of sarcomeric units in fieri in which embryonic protein isoforms are still expressed (more SSTNI than CTNI), which may partially explain why the contractile properties resemble those of fetal myofibrils. Sarcomere structural and functional determinants reflected those recently observed in fetal myocardium (Racca et al., 2015) and other (more)-mature hiPSC-CM cell lines (Lundy et al., 2013) rather than adult ventricular myofibrils (Belus et al., 2010; Racca et al., 2015). Expression of the β-MHC isoform at this stage of maturation explained the similarities in kinetic parameters and that the switch from the α- to β-MHC isoform seen very early in human ventricular myocardial development has already occurred (Racca et al., 2015; Reiser et al., 2001). Moreover, later-stage hiPSC-CMs had cross-bridge kinetics more representative of ventricular versus atrial myofibrils (Belus et al., 2010; Piroddi et al., 2007), where the rate of cross-bridge turnover is faster due to the presence of α-myosin heavy chain (*MYH6* gene). Since the kinetics are similar between myofibrils from hiPSC-CMs and fetal and adult human ventricle muscle, this suggests that in addition to β-myosin, the light chains may also have changed to the ventricular forms. Future studies to test this hypothesis could include an in-depth analysis of myosin light chain isoform composition,

in parallel with heavy chain isoform analysis, as MLC-2v and -2a have been previously proposed as markers for ventricular and atrial differentiation, respectively (Bedada et al., 2014). This may suggest that hiPSC-CMs matured in our conditions develop myofibrils that favor the ventricular rather than the atrial contractile phenotype (Bedada et al., 2014). Thus, myofibril mechanics and kinetic properties may be useful for evaluating the composition of cardiac ventricular versus atrial populations following differentiation, while myofibril contractile properties and sarcomere protein composition may be used as a yardstick for functional maturation that has previously been based primarily on action potential profiles. Our results also point to a note of caution. Despite a misleading adult-like morphology observed by confocal microscopy, the hiPSC-CMs in our study should be considered more as fetal cardiomyocytes in their fine structure and functional capacity, and not be considered as recapitulating the adult cardiomyocyte phenotype.

Since hiPSC-CMs can mature in vitro over time in culture (Lundy et al., 2013), they may prove valuable for investigating the developmental time course of early-stage cardiac diseases, representing a unique platform to predict adverse prenatal outcomes and to develop therapies. We reported FCM hiPSC-CMs carrying the E848G- β-MHC mutation had similar maturation in terms of T-tubule formation but abnormalities at the myofibril level. Myofibril disarray has been described for other *MYH7* mutations and can result from variable expression of mutated and wild-type myosin in individual myocytes, as previously proposed (Kraft et al., 2013). Force decrements result from several *MYH7* mutations (Witjas-Paalberends et al., 2013) and could be due to cardiomyocyte and/or myofibril disarray. Here we demonstrated that, at the individual myofibril level, there is also a force deficit with the E848G β-MHC mutation, which in addition to likely myofibril structural alterations, may be partially due to an accelerated cross-bridge detachment. A pathway similar to the latter was previously suggested for myofibrils from one patient carrying the R403Q β-MHC mutation associated with hypertrophic cardiomyopathy (HCM) (Belus et al., 2008). For the R403Q mutation, an increased cross-bridge detachment rate was related to an increased cost of tension generation (Witjas-Paalberends et al., 2014) and reduced force-generating capacity (Ferrantini et al., 2009). In addition, the development of the sarcomere structure may be delayed or altered during maturation by disease-associated mutations.

Notably, increased Ca^{2+} sensitivity and altered cross-bridge kinetics have been reported as hallmarks of human adult myocardium expressing several *MYH7* mutations (Belus et al., 2008; Witjas-Paalberends et al., 2014). However, in the FCM cell line, structural variability may lead to different amounts of β-myosin heavy chain (and/or total myosin) incorporated into forming myofibrils during maturation, contributing to additional contractile deficits. As a feedback mechanism, weaker tension-generating myofibrils during mechanical loading may lead to cellular hypertrophy during development. We were limited in our ability to quantify sarcomere protein content and concentration in this study, due to the limited amount of the frozen remains of the same myofibril preparations used for the mechanical experiments. Future studies will focus more on documenting the absolute amount of troponin or the relative abundance of SSTNI versus CTNI, as this may affect myofibril Ca^{2+} sensitivity and troponin complex activation (Kreutziger et al., 2011), even if the kinetics of force development or relaxation may be not influenced by the TnI isoform switch (de Tombe et al., 2007).

In conclusion, we were able to assess the structure and function of myofibrils from hiPSC-CMs at a relatively advanced state of maturation, and compared them with properties previously reported for myofibrils from human fetal ventricular muscle. That said, much work remains to be done. We report on only a single time point, thus have not established a developmental time course. In addition, it would be interesting to see if maturation could be further progressed with a longer time in culture or via application of biological molecules such as T3, Let-7 (Kuppusamy et al., 2015; Yang et al., 2014b), or other transcriptional and maturation regulators, or with other environmental conditions such as electrical stimulation and/or varying load. Future studies should also provide more complete and detailed proteomic information regarding the time course of protein isoform appearance, disappearance, stoichiometry of proteins incorporated into myofibrils and post-translational modifications. We have also demonstrated the utility of this approach to study the influence of disease-associated mutations on myofibril structure and function. However, this is just one example of the potential of the approach that can not only be compared with normal development, but also with a myriad of other disease-associated mutations. Finally, while we have provided initial evidence that T-tubule formation may be initiated under our conditions, future studies are needed to verify and extend these results, which may be important for disease studies where calcium handling properties may also be affected and coupled with myofibril dysfunction. Importantly, our approach provides a platform to investigate the earliest stages of disease development resulting from alterations in myofibril properties.

EXPERIMENTAL PROCEDURES

An expanded version of the Experimental Procedures appears in the Supplemental Information.

Human Subjects

Protocols for this study were approved by the Institutional Review Board of the University of Washington. Written consent was obtained from all study participants.

Human Pluripotent Stem Cell Culture and Cardiac Differentiation

Patient-derived cardiomyocytes were differentiated from two healthy volunteers, $control_1$ hiPSC line generated from urine and $control_2$ from skin fibroblasts of healthy patients as well as for the FCM patient hiPSC lines as previously described (Guan et al., 2014). The cardiac myocyte differentiation protocol is described in the Supplemental Experimental Procedures.

Fabrication and Cell Maturation onto a Nanopatterned Substratum

Anisotropically nanofabricated substrata (ANFS) were fabricated using a capillary force lithography procedure as previously described (Kim et al., 2010; Macadangdang et al., 2014). Further details are given in the Supplemental Experimental Procedures.

Cell Morphology, Myofibril Structural, and Protein Analysis

Long-term cultured hiPSC-CM onto nanopatterned surfaces were washed with PBS and in succession fixed with 4% paraformaldehyde, and morphological characteristics were assessed by confocal microscopy. Myofibril structure was assessed by TEM. Sarcomeric protein composition was studied by SDS-PAGE and western blot analysis using frozen remains of myofibril preparations. Details are provided in the Supplement Experimental Procedures.

Myofibrils

Myofibrils were isolated using two separate approaches. One approach provided a greater yield so was used for the majority of experiments. Myofibrils were mounted in a custom-built apparatus, and the mechanical properties measured as previously described (Colomo et al., 1998; Moussavi-Harami et al., 2015; Racca et al., 2015; Tesi et al., 1999). Details are provided in the Supplemental Experimental Procedures.

Statistical Analysis

Data are reported as means ± SEM. Student's two-tailed t test was used with statistical significance in control- and FCM-hiPSC-CM lines set at $*p < 0.05$ and $**p < 0.01$. For controls comparison, one-way ANOVA with a Tukey post hoc test was used with statistical significance set at $p < 0.05$. The number of independent experiments (N) performed was more than three for each analysis. For myofibril mechanics analysis, n = number of myofibrils.

SUPPLEMENTAL INFORMATION

Supplemental Information includes Supplemental Experimental Procedures, two figures, and one table and can be found with this article online at http://dx.doi.org/10.1016/j.stemcr.2016.04.006.

AUTHOR CONTRIBUTIONS

All experiments were performed at the University of Washington in Seattle, WA, USA. J.M.P. designed the method, performed cell differentiation and all experiments, analyzed and interpreted data, and wrote the manuscript. A.W.R. contributed to the myofibril experiments. J.M.K. performed the proteomic assays. K.C.Y. generated the FCM cell line. X.G., D.L.M., and M.K.C. generated and provided the UC 3-4 cell line. L.P. provided training on hiPSC differentiation and $control_2$ cell line. V.M. performed confocal imaging. R.Z. contributed to the cell cultures. J.M. fabricated the ANFS and provided assistance with cell plating. M.Y.J contributed to the design of the myofibril isolation protocol. D.H.K. provided the ANFS. C.P. and C.T. contributed to the design of the myofibril isolation protocol and interpretation of the results. C.E.M. contributed to the overall study design, and provided cells and training assistance. M.R. contributed to the overall study design, interpretation of the results, and writing of the manuscript. All authors critically reviewed the manuscript and approved the final version of this manuscript for publication.

ACKNOWLEDGMENTS

J.M.P. was supported by a "Pegaso" Doctoral Fellowship from the University of Siena, Italy. A.W.R. was supported by F31 from the National Institute of Arthritis and Musculoskeletal and Skin Diseases (NIAMS). J.M.K. was supported by a Heart and Stroke Foundation of Canada Postdoctoral Fellowship. Electron microscopy imaging was done through the Vision Research Center Core at the University of Washington, funded by NIH award number P30 EY01730, with the assistance of Edward Parker. This work was supported by NIH awards HL111197 and HD048895 (M.R.), U01 HL100405, P01 GM081619, R01 HL084642, P01 HL094374, and an award from the Fondation Leducq Transatlantic Network of Excellence (C.E.M.).

Received: November 21, 2015
Revised: April 6, 2016
Accepted: April 7, 2016
Published: May 5, 2016

REFERENCES

Bedada, F.B., Chan, S.S., Metzger, S.K., Zhang, L., Zhang, J., Garry, D.J., Kamp, T.J., Kyba, M., and Metzger, J.M. (2014). Acquisition of a quantitative, stoichiometrically conserved ratiometric marker of maturation status in stem cell-derived cardiac myocytes. Stem Cell Rep. *3*, 594–605.

Belus, A., Piroddi, N., Scellini, B., Tesi, C., D'Amati, G., Girolami, F., Yacoub, M., Cecchi, F., Olivotto, I., and Poggesi, C. (2008). The familial hypertrophic cardiomyopathy-associated myosin mutation R403Q accelerates tension generation and relaxation of human cardiac myofibrils. J. Physiol. *586*, 3639–3644.

Belus, A., Piroddi, N., Ferrantini, C., Tesi, C., Cazorla, O., Toniolo, L., Drost, M., Mearini, G., Carrier, L., Rossi, A., et al. (2010). Effects of chronic atrial fibrillation on active and passive force generation in human atrial myofibrils. Circ. Res. *107*, 144–152.

Colomo, F., Nencini, S., Piroddi, N., Tesi, C., and Poggesi, C. (1998). Calcium dependence of the apparent rate of force generation in single striated muscle myofibrils activated by rapid solution changes. Adv. Exp. Med. Biol. *453*, 373–382.

de Tombe, P.P., Belus, A., Piroddi, N., Scellini, B., Walker, J.S., Martin, A.F., Tesi, C., and Poggesi, C. (2007). Myofilament calcium sensitivity does not affect cross-bridge activation-relaxation kinetics. Am. J. Physiol. Regul. Integr. Comp. Physiol. *292*, R1129–R1136.

Eschenhagen, T., Mummery, C., and Knollmann, B.C. (2015). Modelling sarcomeric cardiomyopathies in the dish: from human heart samples to iPSC cardiomyocytes. Cardiovasc. Res. *105*, 424–438.

Ferrantini, C., Belus, A., Piroddi, N., Scellini, B., Tesi, C., and Poggesi, C. (2009). Mechanical and energetic consequences of HCM-causing mutations. J. Cardiovasc. Transl. Res. *2*, 441–451.

Gazzerro, E., Sotgia, F., Bruno, C., Lisanti, M.P., and Minetti, C. (2010). Caveolinopathies: from the biology of caveolin-3 to human diseases. Eur. J. Hum. Genet. *18*, 137–145.

Gherghiceanu, M., Barad, L., Novak, A., Reiter, I., Itskovitz-Eldor, J., Binah, O., and Popescu, L.M. (2011). Cardiomyocytes derived from human embryonic and induced pluripotent stem cells: comparative ultrastructure. J. Cell Mol. Med. *15*, 2539–2551.

Guan, X., Mack, D.L., Moreno, C.M., Strande, J.L., Mathieu, J., Shi, Y., Markert, C.D., Wang, Z., Liu, G., Lawlor, M.W., et al. (2014). Dystrophin-deficient cardiomyocytes derived from human urine: new biologic reagents for drug discovery. Stem Cell Res. *12*, 467–480.

Jung, G., and Bernstein, D. (2014). hiPSC modeling of inherited cardiomyopathies. Curr. Treat Options Cardiovasc. Med. *16*, 320.

Kamakura, T., Makiyama, T., Sasaki, K., Yoshida, Y., Wuriyanghai, Y., Chen, J., Hattori, T., Ohno, S., Kita, T., Horie, M., et al. (2013). Ultrastructural maturation of human-induced pluripotent stem cell-derived cardiomyocytes in a long-term culture. Circ. J. *77*, 1307–1314.

Kim, D.H., Lipke, E.A., Kim, P., Cheong, R., Thompson, S., Delannoy, M., Suh, K.Y., Tung, L., and Levchenko, A. (2010). Nanoscale cues regulate the structure and function of macroscopic cardiac tissue constructs. Proc. Natl. Acad. Sci. USA *107*, 565–570.

Kraft, T., Witjas-Paalberends, E.R., Boontje, N.M., Tripathi, S., Brandis, A., Montag, J., Hodgkinson, J.L., Francino, A., Navarro-Lopez, F., Brenner, B., et al. (2013). Familial hypertrophic cardiomyopathy: functional effects of myosin mutation R723G in cardiomyocytes. J. Mol. Cell Cardiol. *57*, 13–22.

Kreutziger, K.L., Piroddi, N., McMichael, J.T., Tesi, C., Poggesi, C., and Regnier, M. (2011). Calcium binding kinetics of troponin C strongly modulate cooperative activation and tension kinetics in cardiac muscle. J. Mol. Cell Cardiol. *50*, 165–174.

Kuppusamy, K.T., Jones, D.C., Sperber, H., Madan, A., Fischer, K.A., Rodriguez, M.L., Pabon, L., Zhu, W.Z., Tulloch, N.L., Yang, X., et al. (2015). Let-7 family of microRNA is required for maturation and adult-like metabolism in stem cell-derived cardiomyocytes. Proc. Natl. Acad. Sci. USA *112*, E2785–E2794.

Liu, J., Sun, N., Bruce, M.A., Wu, J.C., and Butte, M.J. (2012). Atomic force mechanobiology of pluripotent stem cell-derived cardiomyocytes. PLoS One *7*, e37559.

Lundy, S.D., Zhu, W.Z., Regnier, M., and Laflamme, M.A. (2013). Structural and functional maturation of cardiomyocytes derived from human pluripotent stem cells. Stem Cells Dev. *22*, 1991–2002.

Macadangdang, J., Lee, H.J., Carson, D., Jiao, A., Fugate, J., Pabon, L., Regnier, M., Murry, C.E., and Kim, D.H. (2014). Capillary force lithography for cardiac tissue engineering. J. Vis. Exp. http://dx.doi.org/10.3791/50039.

Macadangdang, J., Guan, X., Smith, A.S., Lucero, R., Czerniecki, S., Childers, M.K., Mack, D.L., and Kim, D.H. (2015). Nanopatterned human iPSC-based model of a dystrophin-null cardiomyopathic phenotype. Cell. Mol. Bioeng. *8*, 320–332.

Moussavi-Harami, F., Razumova, M.V., Racca, A.W., Cheng, Y., Stempien-Otero, A., and Regnier, M. (2015). 2-Deoxy adenosine triphosphate improves contraction in human end-stage heart failure. J. Mol. Cell Cardiol. *79*, 256–263.

Palpant, N.J., Pabon, L., Roberts, M., Hadland, B., Jones, D., Jones, C., Moon, R.T., Ruzzo, W.L., Bernstein, I., Zheng, Y., et al. (2015). Inhibition of beta-catenin signaling respecifies anterior-like endothelium into beating human cardiomyocytes. Development *142*, 3198–3209.

Parton, R.G., Way, M., Zorzi, N., and Stang, E. (1997). Caveolin-3 associates with developing t-tubules during muscle differentiation. J. Cell Biol. *136*, 137–154.

Pasek, M., Simurda, J., Christé, G., and Orchard, C.H. (2008). Modelling the cardiac transverse-axial tubular system. Prog. Biophys. Mol. Biol. *96*, 226–243.

Piroddi, N., Belus, A., Scellini, B., Tesi, C., Giunti, G., Cerbai, E., Mugelli, A., and Poggesi, C. (2007). Tension generation and relaxation in single myofibrils from human atrial and ventricular myocardium. Pflugers Arch. *454*, 63–73.

Poggesi, C., and Ho, C.Y. (2014). Muscle dysfunction in hypertrophic cardiomyopathy: what is needed to move to translation? J. Muscle Res. Cell Motil. *35*, 37–45.

Poggesi, C., Tesi, C., and Stehle, R. (2005). Sarcomeric determinants of striated muscle relaxation kinetics. Pflugers Arch. *449*, 505–517.

Racca, A.W., Klaiman, J.M., Pioner, J.M., Cheng, Y., Beck, A.E., Moussavi-Harami, F., Bamshad, M.J., and Regnier, M. (2015). Contractile properties of developing human fetal cardiac muscle. J. Physiol. *594*, 437–452.

Reiser, P.J., Portman, M.A., Ning, X.-H., and Moravec, C.S. (2001). Human cardiac myosin heavy chain isoforms in fetal and failing adult atria and ventricles. Am J. Physiol. Heart Circ. Physiol. *280*, H1814–H1820.

Ribeiro, M.C., Tertoolen, L.G., Guadix, J.A., Bellin, M., Kosmidis, G., D'Aniello, C., Monshouwer-Kloots, J., Goumans, M.J., Wang, Y.L., Feinberg, A.W., et al. (2015). Functional maturation of human pluripotent stem cell derived cardiomyocytes in vitro–correlation between contraction force and electrophysiology. Biomaterials *51*, 138–150.

Rodriguez, A.G., Han, S.J., Regnier, M., and Sniadecki, N.J. (2011). Substrate stiffness increases twitch power of neonatal cardiomyocytes in correlation with changes in myofibril structure and intracellular calcium. Biophys. J. *101*, 2455–2464.

Rodriguez, M.L., Graham, B.T., Pabon, L.M., Han, S.J., Murry, C.E., and Sniadecki, N.J. (2014). Measuring the contractile forces of human induced pluripotent stem cell-derived cardiomyocytes with arrays of microposts. J. Biomech. Eng. *136*, 051005.

Sacconi, L., Ferrantini, C., Lotti, J., Coppini, R., Yan, P., Loew, L.M., Tesi, C., Cerbai, E., Poggesi, C., and Pavone, F.S. (2012). Action potential propagation in transverse-axial tubular system is impaired in heart failure. Proc. Natl. Acad. Sci. USA *109*, 5815–5819.

Sasse, S., Brand, N.J., Kyprianou, P., Dhoot, G.K., Wade, R., Arai, M., Periasamy, M., Yacoub, M.H., and Barton, P.J. (1993). Troponin I gene expression during human cardiac development and in end-stage heart failure. Circ. Res. *72*, 932–938.

Stehle, R., Solzin, J., Iorga, B., and Poggesi, C. (2009). Insights into the kinetics of Ca2+-regulated contraction and relaxation from myofibril studies. Pflugers Arch. *458*, 337–357.

Sun, N., Yazawa, M., Liu, J., Han, L., Sanchez-Freire, V., Abilez, O.J., Navarrete, E.G., Hu, S., Wang, L., Lee, A., et al. (2012). Patient-specific induced pluripotent stem cells as a model for familial dilated cardiomyopathy. Sci. Transl. Med. *4*, 130ra147.

Synnergren, J., Ameen, C., Jansson, A., and Sartipy, P. (2012). Global transcriptional profiling reveals similarities and differences between human stem cell-derived cardiomyocyte clusters and heart tissue. Physiol. Genomics *44*, 245–258.

Tesi, C., Colomo, F., Nencini, S., Piroddi, N., and Poggesi, C. (1999). Modulation by substrate concentration of maximal shortening velocity and isometric force in single myofibrils from frog and rabbit fast skeletal muscle. J. Physiol. *516*, 847–853.

Tulloch, N.L., Muskheli, V., Razumova, M.V., Korte, F.S., Regnier, M., Hauch, K.D., Pabon, L., Reinecke, H., and Murry, C.E. (2011). Growth of engineered human myocardium with mechanical loading and vascular coculture. Circ. Res. *109*, 47–59.

van den Berg, C.W., Okawa, S., Chuva de Sousa Lopes, S.M., van Iperen, L., Passier, R., Braam, S.R., Tertoolen, L.G., del Sol, A., Davis, R.P., and Mummery, C.L. (2015). Transcriptome of human foetal heart compared with cardiomyocytes from pluripotent stem cells. Development *142*, 3231–3238.

Witjas-Paalberends, E.R., Piroddi, N., Stam, K., van Dijk, S.J., Oliviera, V.S., Ferrara, C., Scellini, B., Hazebroek, M., ten Cate, F.J., van Slegtenhorst, M., et al. (2013). Mutations in MYH7 reduce the force generating capacity of sarcomeres in human familial hypertrophic cardiomyopathy. Cardiovasc. Res. *99*, 432–441.

Witjas-Paalberends, E.R., Ferrara, C., Scellini, B., Piroddi, N., Montag, J., Tesi, C., Stienen, G.J., Michels, M., Ho, C.Y., Kraft, T., et al. (2014). Faster cross-bridge detachment and increased tension cost in human hypertrophic cardiomyopathy with the R403Q MYH7 mutation. J. Physiol. *592*, 3257–3272.

Yang, X., Pabon, L., and Murry, C.E. (2014a). Engineering adolescence: maturation of human pluripotent stem cell-derived cardiomyocytes. Circ. Res. *114*, 511–523.

Yang, X., Rodriguez, M., Pabon, L., Fischer, K.A., Reinecke, H., Regnier, M., Sniadecki, N.J., Ruohola-Baker, H., and Murry, C.E. (2014b). Tri-iodo-l-thyronine promotes the maturation of human cardiomyocytes-derived from induced pluripotent stem cells. J. Mol. Cell Cardiol. *72*, 296–304.

Stem Cell Reports, Volume *6*

Supplemental Information

Isolation and Mechanical Measurements of Myofibrils from Human Induced Pluripotent Stem Cell-Derived Cardiomyocytes

Josè Manuel Pioner, Alice W. Racca, Jordan M. Klaiman, Kai-Chun Yang, Xuan Guan, Lil Pabon, Veronica Muskheli, Rebecca Zaunbrecher, Jesse Macadangdang, Mark Y. Jeong, David L. Mack, Martin K. Childers, Deok-Ho Kim, Chiara Tesi, Corrado Poggesi, Charles E. Murry, and Michael Regnier

SUPPLEMENT

Supplemental figure legends

Supplemental Figure 1. Later-stage hiPSC-CMs grown on nanopatterned surfaces showed myofibril disarray, cellular hypertrophy but same resting sarcomere lenght. Confocal images of late-stage FCM-hiPSC-CMs grown nanopatterned surfaces. Cells were stained for Z-bands (α-actinin, red) and for the nuclei (DAPI, blue). In FCM-hiPSC-CMs, Z-bands alignment signs pronounced myofibrillar disarray ($n_{Control}$ = 16; n_{FCM} =5). Cell area, based on myofibril composition, exhibited cellular hypertrophy ($n_{Control}$ = 100; n_{FCM} =34). Resting sarcomere length was 1.8 µm as for Controls, p=0.714 ($n_{Control}$ = 10; n_{FCM} =7). N>3 for each cell line. *p<0.05; **p<0.01; # not significant. Scale bars equal to 20 µm**.**

Supplemental Figure 2. Later-stage hiPSC-CMs grown on nanopatterned surfaces showed myofibril disarray, cellular hypertrophy but still have T-tubule formation. Confocal images of FCM-hiPSC-CMs stained with antibody anti-CAV3 (green), anti-α-actinin (red) and nuclei (DAPI, blue). Side view (100% of magnification) of merged image of representative of FCM-hiPSC-CMs displayed axial tubular elements (green), running perpendicular to Z-bands (red), similar to Control-hiPSC-CMs (Fig.2). Transverse tubules (green) covered the entire cell surface and appear parallel to the Z-lines. Scale bars equal to 20 µm.

Supplemental Table 1. Summary of mechanical and kinetic properties of myofibrils from Control-hiPSC-CM line following maximal and submaximal Ca^{2+} activation. Data from each group of Controls was compared with ANOVA and a Tukey post-hoc test with statistical significance set at p<0.05. No significant differences were found between Controls. For comparisons, $Control_1$ and $Control_2$ data were merged in Table 1. (n) equal to number of myofibrils. N=3 for each condition.

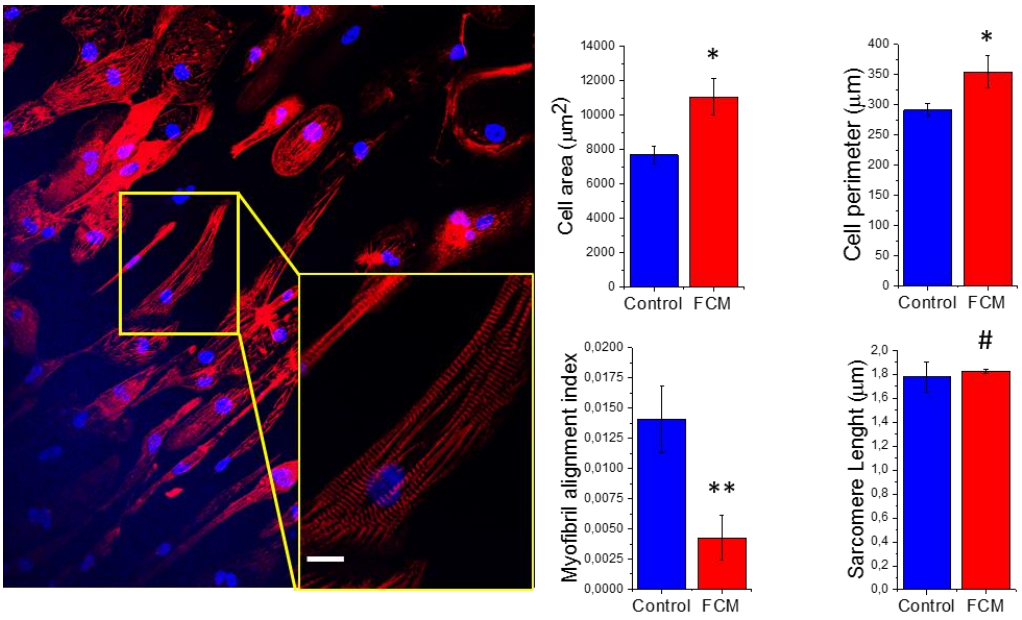

Supplemental Figure 1

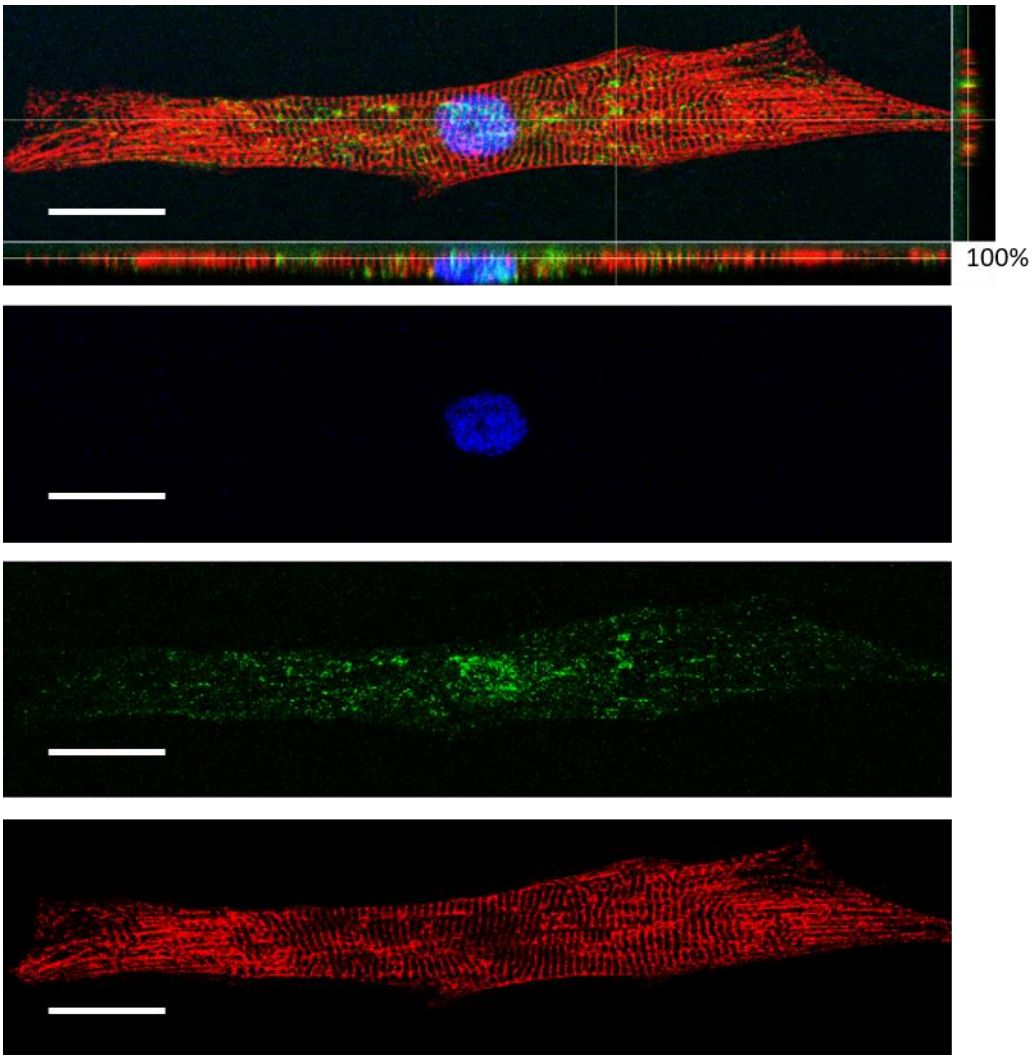

Supplemental Figure 2

Supplemental Table 1

Myofibril type	Tension	k_{ACT}	k_{REL}, slow	t_{REL}, slow	k_{REL}, fast
pCa 4.0	**mN/mm^2**	**s^{-1}**	**s^{-1}**	**ms**	**s^{-1}**
Control$_1$	19.4±3.4 (14)	0.65±0.07 (12)	0.28±0.04 (13)	202±10 (15)	2.36±0.3 (14)
Control$_2$	15.2±3.3 (12)	0.47±0.05 (11)	0.31±0.06 (12)	181±38 (14)	2.15±0.1 (11)
p value	0.68	0.07	0.71	0.16	0.41
pCa 5.8					
Control$_1$	10.1±2 (13)	0.40±0.06 (13)	0.28±0.03 (9)	154±14 (11)	1.98±0.4 (13)
Control$_2$	6.2±1.8 (9)	0.37±0.11 (9)	0.44±0.07 (8)	154±6 (10)	1.87±0.2 (9)
p value	0.19	0.84	0.06	0.99	0.15

Supplemental experimental procedures

Human pluripotent stem cell culture and cardiac differentiation

For cardiac differentiation we applied an established monolayer directed differentiation protocol(Palpant et al., 2015). In brief, hiPSC are grown in serum-free conditions until a confluent monolayer of cells seeded onto Matrigel-coated (Fisher) wells appears as compact at 37°C, 5% CO_2. One day before cardiac differentiation induction, the Wnt signaling pathway agonist Chiron 99021 (1µM) was applied. On day 0, the directed differentiation is started by adding Activin A (100 ng/ml, R&D) for 18 hours. On day 1, medium was supplemented with bone morphogenetic protein-4 (BMP4, 5 ng/ml, R&D) and Chiron 99021 until day 3 when replaced with Wnt antagonist Xav 939 (1µM). From day 0 to day 7 the base media is composed of RPMI supplemented with B27 minus insulin (Invitrogen). From day 7 onwards, cultures were fed every other day with RPMI medium with B27 supplement (Invitrogen). Spontaneous beating monolayers are generally noticeable from day 8 from Activin A induction onwards. On day 20 post differentiation, single cells are obtained from beating monolayers for further cardiac maturation. Monolayers more than 60% positive for cardiac troponin T by flow cytometry were used for subsequent experiments.

Fabrication and cell maturation onto a nanopatterned substratum

A nanopatterned silicon master was used as template for a polyurethane acrylate (PUA) mold used to pattern a polyurethane (PU)-based polymer via UV-assisted CFL. The PUA master mold used for our purpose was designed with parallel grooves and ridges of 800 nm wide and 500nm deep. PU pre-polymer is drop dispensed onto a glass coverslip (18mm diameter, Fisher) and the PUA mold is placed on top. For photopolymerization, the mold was cured via UV radiation (wavelength of 250-400nm) and then peeled off leaving behind an ANFS for cell culture. For the maturation process, single cells were replated at low density (10,000 cells/cm^2) onto fibronectin coated nanopatterned surfaces (5µg/cm^2) and long-term cultured (80 days for myofibril isolation, 80-100 for structural analysis, average 88.1±2.9 days). For mechanical studies and structural analysis, only FCM-CMs were frozen beforehand at day 50 onto nanopatterned surfaces and then matured for other 30 days with the same procedure after thawing. For proteomic analysis, single Control- and FCM-CMs were matured onto flat surfaces and frozen at day 50. After thawing, cells were matured onto nanopatterned surfaces for additional 30 days. Cultures were monitored daily for cell spreading and physiological hypertrophy.

Immunocytochemistry

Long-term cultured cells onto nanopatterned surfaces were washed with PBS and in succession fixed with 4% paraformaldehyde in PBS for 20 minutes at room temperature. For Z-bands staining, cells were blocked in 1.5% normal goat serum with Triton X-100 0.1% for 30 minutes and then incubated with anti-α-actinin primary antibody 1:800 (A7811, Sigma) at 4°C overnight. After PBS rinses, samples were stained with Alexa Fluor 594 goat anti-mouse secondary antibody 1:100 (A-11005, Life Technologies) for 1 hour at room temperature. For caveolin-3 (CAV3), cells were incubated with 1.5% normal goat serum before labeling with anti-CAV3 primary antibody 1:500 (AV09021, Sigma) and the day after with Alexa Fluor 488 goat anti-rabbit 1:200 (A-11008, Life Technologies). Each staining with secondary antibody was incubated for 1 hour and later PBS washed prior to nuclei staining with DAPI (Vectashield). Nanopatterned coverslides were then flipped over a normal miscroscope slide for confocal images (Nikon A1R confocal microscope).

Imaging and morphological analysis

Images captured by confocal microscope were analyzed for average cell area, cell perimeter and sarcomere length (SL) in Fijii (ImageJ) Software using standard analysis plugin. Myofibril alignment resulted from Z-bands density and bidimensional organization was analyzed using an algorithm based on the Fast Fourier Transform (FFT) similarly to previously described method(Ferrantini et al., 2014). Single cells were discernible from each other for the quantification of myofibril alignment. The periodicity of Z-bands along the entire cell surface were reflected in the peak components of the power spectrum profile. The area of the first order of spatial frequency components centered at 0.55±0.05 corresponding to the measured resting SL was normalized for the entire area under the power spectrum curve. The resulted value is as much greater as the myofibril alignment index of each single cell.

Transmission electron microscopy

Single hiPSC-CMs onto nanopatterned surfaces were fixed in 4% glutaraldehyde in sodium cacodylate buffer overnight at 4°C, washed and then post fixed in 2% Osmium Tetroxide for 1 hour on ice. Following Osmium, samples were washed in water and block stained in 2% Uranyl Acetate, washed again and dehydrated through a series of ethanol. Finally, they were infiltrated and embedded in Epon Araldite. Ultrathin (70-80 nm) axial sections of single cells were contrasted with lead citrate prior to imaging with a JEOL JEM 1200EXII at 80 kV.

Myofibril protein analysis

Sarcomeric protein composition was studied using frozen remains of myofibril preparations. Myofibril sediments were centrifuged at 10,000 RPM and supernatant taken off the top. Protein suspension was then solubilized in SDS-loading buffer, sonicated 3*30seconds on ice and then boiled for 4 min. Samples were separated on 10% or 12% SDS-PAGE gels using a Mini-PROTEAN® Tetra Cell (Bio-Rad Laboratories). The SDS-PAGE gel was transferred onto a PVDF membrane using the Mini-PROTEAN® Tetra Cell wet transfer system (Bio-Rad Laboratories). The primary antibodies used were as follows; TNI 1:2500 (sc-15368, Santa Cruz), CTNT 1:2500 (C-19, sc8121, Santa Cruz), α-ACTIN 1:5000 (A1203, Santa Cruz) and β-MHC (1:5000), Secondary antibody 1:10,000. β-MHC expression was tested to provide evidence that the presence of slow β-MHC isoform may be responsible for similarities in kinetics of myofibrils from hiPSC-CMs, fetal human and adult human cells (Fig. 3D), while expression of the embryonic SSTNI or cTNI isoforms can be used as markers for maturation.

Isolation of myofibrils

A cell length of >50 µm in most of the culture was used as parameter for evaluate myofibril elongation state. Myofibrils were isolated using two different approaches. In the *skinning in suspension* approach, cells were fed including Rho Kinase (ROCK) inhibitor (1:1000) and incubated for 1 hour. After PBS rinse, cells were incubated again in Versene for 1 hour. Detached cells were gently resuspended into rigor solution (KCl 100 mM, $MgCl_2$ 2 mM, EGTA 1 mM, Tris-HCl 50 mM, pH 7.0) supplemented with protease inhibitor cocktail 5 µl/ml and DTT 2 µl/ml (Sigma) and 1% Triton X for 5 minutes on ice after rapid vortexing for the skinning process. Samples were spun at 3000 rpm for other 5 minutes and the pellet was resuspended into fresh supplemented rigor solution without Triton X. Two consecutive rinses were performed as described in the previous step. In the *skinning on plate* approach, cells were PBS washed before direct treatment with skinning solution for 5 minutes on ice. Supernatant containing cells under skinning was collected and processed as described

for the first approach. Myofibril suspensions were stored at 4°C for mechanical experiments and used for 1-2 days.

Solutions for mechanical measurements

Experimental solutions for myofibril mechanics were calculated as previously described(Brandt et al., 1998). Experimental solutions were composed as follows (in mM): phosphocreatine 10, EGTA 10 (ratio of CaEGTA/EGTA set to obtain Ca^{2+} values between 10^{-9} and 10^{-4} M), MOPS 10, free Mg^{2+} 1, (Na^{+} + K^{+}) 155, MgATP 5, and propionate and sulphate to adjust the final solution ionic strength to 0.2 M. Both solutions were adjusted to pH 7.0 with NaOH.

Myofibril mechanics

Myofibril were mounted in a custom built apparatus and measured in the mechanical properties as previously described(Colomo et al., 1998; Moussavi-Harami et al., 2015; Racca et al., 2015; Tesi et al., 1999). Single or bundles of few myofibrils were mounted between the tip of two needles micro-forged from borosiliacate glass capillary tubes (OD 1.0 mm, ID 0.5 mm, Sutter Instruments, Novato, CA, USA) (Fig. 3A right). One of the two glass microneedles that held the myofibrils was relatively stiff and was mounted on the lever arm of a piezo-controller motor (PZT Servo controller, LVPZT amplifier; Physik Instrumente, Irvine, CA, USA). In these experimental conditions, the compliance of the force transducer microneedle was 44.15±8.5 nN μm^{-1}. The flexibility of the arm of the needle was calibrated with a given force by increasing the frequency of a galvanometer and measuring its deflection under 40x lens as previously described(Colomo et al., 1998). The tip of the force transducer was blackened with ink in order to increase the sensitivity of the photosensor. During the experiment, the force transducer was positioned over a photodiode system which detect the displacement of the needle that correlates to the force development of the myofibril(Cecchi et al., 1993). The flow of relaxing and the activating solution streamed by gravity from a double-barrelled borosilicate theta glass pipette (Capillary glass tubing OD 2.0 mm, ID 1.4 mm, SEP 0.2 mm, modified in house to OD of 0.55 mm, Warner Instruments, Hamden, CT, USA) and was controlled by a computerized motor for switching the solution over the preparation in about 10 ms (SF-77B Perfusion Fast step, Warner Instruments Corporation, Hamden, CT, USA). The initial SL of the attached myofibril was set at 2.34 µm that corresponded about 15% above the slack length(Tesi et al., 1999). The time course of activation and relaxation kinetics were collected constantly at 15°C(Kreutziger et al., 2011)(Fig. 4A). Maximal (pCa 4.0) and submaximal (pCa 5.8) isometric tension generation was calculated from the force amplitude and normalized for the cross sectional area of the myofibril. The rate of tension generation (k_{ACT}) follows Ca^{2+} application and was estimated from monoexponential fits. The rate of the slow phase of relaxation (slow k_{REL}) is calculated from the slope of a regression line fitted to the tension trace and normalized to the entire amplitude of the tension relaxation trace. The duration of slow phase (slow t_{REL}) was estimated from the onset of the linear slope to the beginning of the shoulder leading to the fast phase of relaxation. The relaxation rate for the fast phase (fast k_{REL}) was measured from the monoexponential decay fitted to the data. The time to generate or reduce half-maximal force ($t_{1/2}$) was used for calculate k_{ACT} and fast k_{REL} and converted to a rate $\tau = \ln(2)/t_{1/2}$.

Supplemental references

Brandt, P.W., Colomo, F., Piroddi, N., Poggesi, C., and Tesi, C. (1998). Force regulation by Ca^{2+} in skinned single cardiac myocytes of frog. Biophysical Journal *74*, 1994-2004.

Cecchi, G., Colomo, F., Poggesi, C., and Tesi, C. (1993). A force transducer and a length-ramp generator for mechanical investigations of frog-heart myocytes. Pflugers Arch *423*, 113-120.

Ferrantini, C., Coppini, R., Sacconi, L., Tosi, B., Zhang, M.L., Wang, G.L., de Vries, E., Hoppenbrouwers, E., Pavone, F., Cerbai, E., *et al.* (2014). Impact of detubulation on force and kinetics of cardiac muscle contraction. J Gen Physiol *143*, 783-797.